

Accelerated Discovery of Thermoelectric Materials: Combinatorial Facility and High-Throughput Measurement of Thermoelectric Power Factor

Jorge García-Cañadas,^{†,||} Nicholas J. E. Adkins,[‡] Stephen McCain,[‡] Bastian Hauptstein,[‡] Ashley Brew,[†] David J. Jarvis,[§] and Gao Min^{*,†}

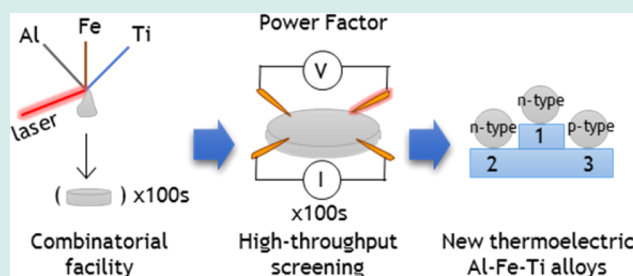
[†]School of Engineering, Cardiff University, The Parade, Cardiff CF24 3AA, United Kingdom

[‡]College of Engineering & Physical Sciences, The University of Birmingham, Edgbaston, Birmingham B15 2TT, United Kingdom

[§]European Space Agency, Keplerlaan 1, PO Box 299, 2200 AG Noordwijk, The Netherlands

ABSTRACT: A series of processes have been developed to facilitate the rapid discovery of new promising thermoelectric alloys. A novel combinatorial facility where elements are wire-fed and laser-melted was designed and constructed. Different sample compositions can be achieved by feeding different element wires at specific rates. The composition of all the samples prepared was tested by energy dispersive X-ray spectroscopy (EDS). Then, their thermoelectric properties (power factor) at room temperature were screened in a specially designed new high-throughput setup. After the screening, the thermoelectric properties can be mapped with the possibility of identifying compositional trends. As a proof-of-concept, a promising thermoelectric ternary system, Al–Fe–Ti, has been identified, demonstrating the capability of this accelerated approach.

KEYWORDS: high-throughput, thermoelectric materials, laser processing, combinatorial chemistry, power factor



INTRODUCTION

Nowadays, there is an increasing demand on power generation. In this respect, thermoelectricity has attracted considerable interest over the past decades due to its ability to directly convert heat into electricity and its application in solid-state refrigeration.¹ Most of the research on developing new materials has been focused on maximizing the dimensionless figure of merit ZT , which relates to the efficiency of the materials. It is defined as $ZT = S^2T/\lambda\rho$, where S is the Seebeck coefficient, T the absolute temperature, λ the thermal conductivity, and ρ the electrical resistivity. The power factor, defined as S^2/ρ , is also a useful parameter to evaluate thermoelectric performance of materials.

There is a strong demand on high- ZT bulk materials, specially containing environmentally friendly, sustainable and abundant elements.² The search for new thermoelectric materials requires huge amounts of sample synthesis and characterization. For this reason, combinatorial approaches are of significant importance for accelerating the discovery of novel materials.³ Examples of both experimental^{4–7} and theoretical approaches^{8–11} have been reported in the literature. Employing this approach, a wide number of compounds combining different elements in a wide range of compositions can be synthesized. Then, the relevant properties have to be measured by means of high-throughput facilities, leading to a library of compositional-dependent properties useful to identify promising materials and find out compositional trends.

Here we report an integral combinatorial approach where a vast number of bulk alloy samples have been prepared in a novel combinatorial facility fed by wires of different pure elements. The wires were laser-melted to form the alloys and 52 different compositions were achieved by adapting the feed rate of each wire. The thermoelectric power factor was then screened at room temperature in all the samples using a specially designed high-throughput facility. After an initial screening of hundreds of different samples, a promising ternary system, Al–Fe–Ti was identified.

EXPERIMENTAL PROCEDURES

Combinatorial Facility. This facility is based on the suspended droplet alloying (SDA) concept, which utilizes a laser beam to melt elemental wire feedstock in order to produce a small button of bulk alloy material (see Figure 1). Compositionally different samples can be synthesized by varying the ratio of wire feed rates. The alloying process begins when the aligned wires from each element are fed into the beam path and melt. The melting process initiates the formation of a droplet on the tip of each wire. The elemental droplets grow as new material is fed into them. Because of the proximity of the wires to one another, the droplets join and

Received: November 25, 2015

Revised: April 28, 2016

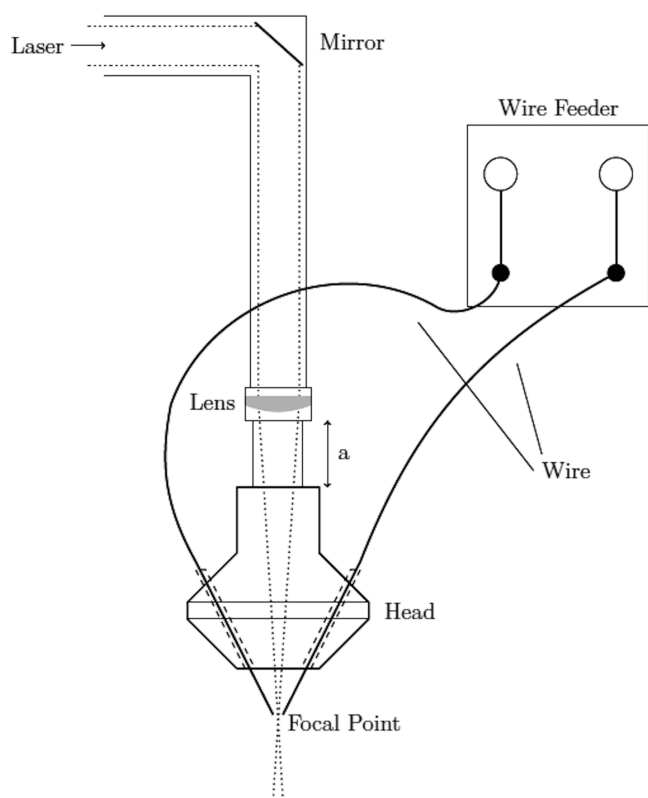


Figure 1. Schematic of wire fed suspended droplet alloying process (not to scale).

72 form a single alloy droplet, which is suspended only by the
 73 wires feeding into it. The droplet remains suspended on the tip
 74 of the wires due to surface tension. Once the mass of the
 75 droplet becomes large enough, the gravity force overcomes the
 76 force of surface tension and the droplet detaches from the wires
 77 falling onto the substrate. As more of these alloy droplets are
 78 deposited, the bottom of the sample begins to freeze. However,
 79 it is still possible to maintain a molten pool in the upper region
 80 of the sample. This droplet deposition sequence is repeated a

number of times until the desired sample height is achieved; at
 81 which point the laser and wire feeders are simultaneously
 82 stopped. The sample is then allowed to cool under argon
 83 shielding gas with a flow rate of 5 L/min. The whole process is
 84 performed in an argon filled glovebox with oxygen levels of 30
 85 ppm or less.

The key to the SDA process lies in the ability to mix and
 87 alloy relatively small volumes of material while it is in contact
 88 with only its constituent parts (the elemental wires). SDA is
 89 achieved through precise alignment of the wires with one
 90 another in a region where they will intersect the beam path and
 91 melt. The wire alignment encourages the elemental droplets to
 92 join and mix with one another shortly after their formation.
 93 Precise control of the wire feed rates and the 100% capture rate
 94 of material allows an alloy with the desired stoichiometry to be
 95 produced with a high degree of accuracy.

Feedstock material was purchased from Advent Research
 97 Materials (UK). For the case of Al, Fe, and Ti, 1 mm diameter
 98 wires with 99.8% purity or higher were used. The substrate
 99 material, where the alloy droplets were deposited, was
 100 produced from 430-grade stainless steel disc 20 mm in
 101 diameter with a thickness of 2 mm. Before alloy synthesis
 102 could be commenced some preparatory steps were performed.
 103 The wires required to synthesize the thermoelectric alloy were
 104 weighed on a four-point balance to ascertain the mass in terms
 105 of a linear density (g/m). This allows a target composition in
 106 atomic percentage (at. %) to be calculated to a ratio of wire
 107 feed rates (mm/min) for individual wires.

The wires required to produce the bulk material were loaded
 109 into the wire feeder assemblies, inserted into a copper delivery
 110 nozzle and aligned within the beam path. The feed rates (mm/
 111 min) required to produce the specific target composition were
 112 calculated and entered into the control software for each wire
 113 feeder. A substrate was positioned underneath the copper
 114 delivery nozzle in the center of the beam path on a *X,Y* table. A
 115 laser power sufficient to melt the wires at the specified feed
 116 rates was selected. The laser beam was then fired in continuous
 117 wave mode and the wire feeders were activated. Samples are
 118 typically produced in 2 min.

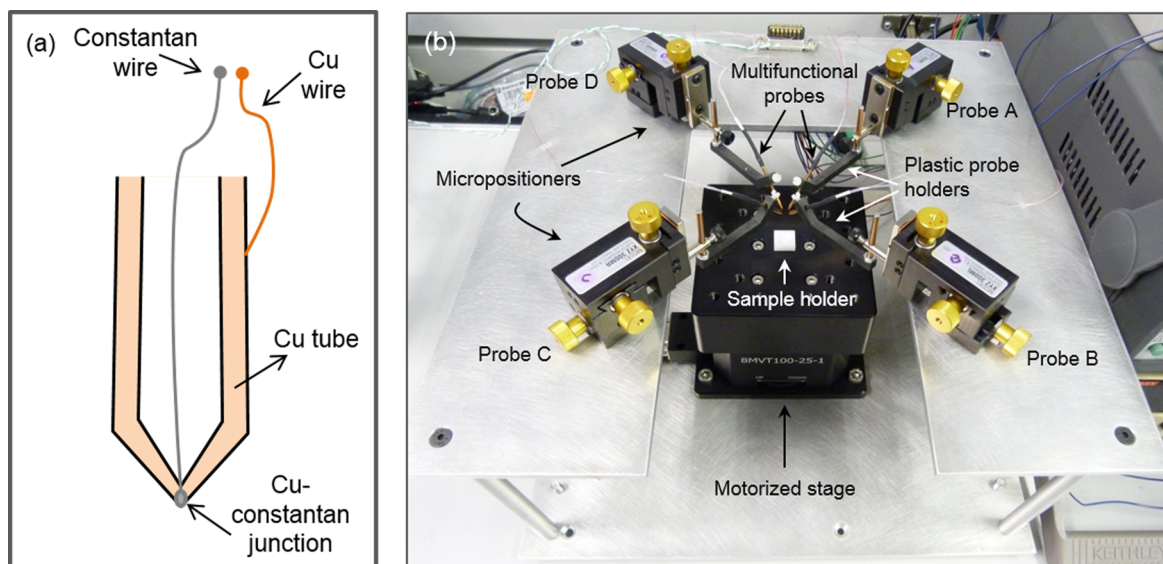


Figure 2. (a) Scheme of the components of a multifunctional probe. (b) Picture of the power factor screening facility.

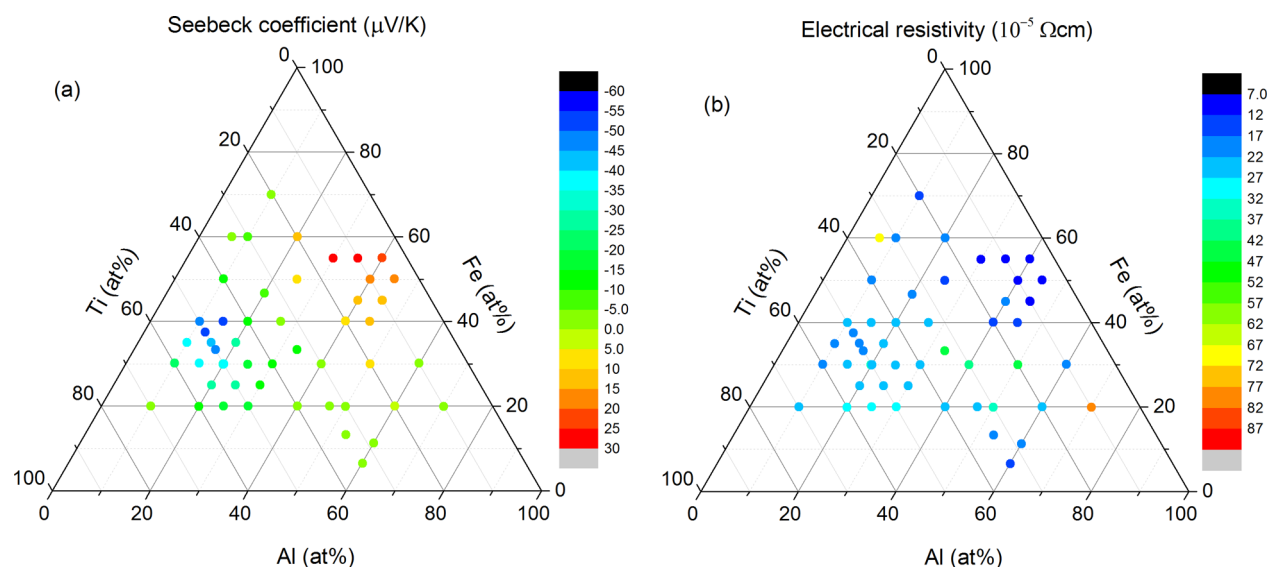


Figure 3. Thermoelectric screening of the Al–Fe–Ti ternary alloys: (a) the Seebeck coefficient and (b) electrical conductivity.

120 For the screening of the thermoelectric properties the
 121 samples were cut to a 1–2 mm thick disc perpendicular to the
 122 build direction using an AgieCharmilles Cut 20 EDM. This disc
 123 was then ground and polished. Discs diameter varied from 6 to
 124 15 mm. Sample composition was confirmed using a Hitachi
 125 TM3000 Desktop Scanning Electron Microscope (SEM) with
 126 Bruker XFlash 4010 Energy Dispersive X-ray Spectroscopy
 127 (EDS) detector in conjunction with Bruker Quantax Esprit 1.9
 128 software. An agreement of $\pm 2\%$ respect to the compositions
 129 from the feed was found. No compositional gradients were
 130 identified from EDS measurements performed at different
 131 surface points on the sample discs Phase identification was
 132 performed in selected samples by X-ray diffraction (XRD)
 133 using a Phillips PW1710 Automated Powder Diffractometer
 134 with copper (Cu $K\alpha$) radiation at 35 kV and 40 mA. The
 135 diffractometer was controlled with PW1877 APD version 3.6
 136 computer software and initial phase identification was
 137 performed using PW1876 PC-Identif version 1.0b software.
 138 XRD samples were prepared by grinding the discs with a pestle
 139 and mortar to a powder and packing them into an aluminum
 140 holder.

141 **High-Throughput Power Factor Measurement Fa-**
 142 **tility.** The measurement of the power factor involves the
 143 determination of both Seebeck coefficient and electrical
 144 resistivity. Unlike thermal conductivity, the power factor can
 145 be measured quicker and has been chosen as the main indicator
 146 for the initial screening of the thermoelectric performance.
 147 Examples of high-throughput tools for the measurement of
 148 power factor can be found in the literature, most of them
 149 focused on thin films.^{5,7,12,13} Although it can also be used for
 150 thin films, the facility we developed for the screening of the
 151 power factor was designed for bulk samples. The details of the
 152 apparatus have been recently reported.¹⁴ As a summary, the
 153 equipment measures the electrical resistivity using the Van der
 154 Pauw method¹⁵ and the Seebeck coefficient is measured by
 155 means of a hot probe. The key aspect of the facility is the use of
 156 4 multifunctional probes. Each multifunctional probe consists
 157 of a Cu tube with a constantan wire welded right at the tip,
 158 forming a T-type thermocouple as shown in Figure 2a. In this
 159 way, the temperature can be measured right at each probe tip

and the Cu part can be used to provide electrical contacts for
 the flow of current and the measurement of voltages.

For the measurement the sample was first placed on a sample
 holder fixed on a motorized stage (Figure 2b). Then, the stage
 was lifted and the 4 multifunctional probes were contacted at
 the edges of the sample, as required by the Van der Pauw
 method. Inside probe A, a heater coil was installed to set its
 temperature ~ 3 K above room temperature to allow Seebeck
 coefficient measurements. By consecutively measuring the
 temperatures at the tips of probes A (T_A) and D (T_D), and
 the open-circuit voltage difference (ΔV) across them through
 their Cu wires, the Seebeck coefficient of the sample was
 calculated as $S = \Delta V / (T_A - T_D) + S_{Cu}$ (S_{Cu} is the Seebeck
 coefficient of the Cu used in the multifunctional probes¹⁴). The
 electrical resistivity was measured directly afterward (keeping
 probe A hot) by applying current across two adjacent probes
 and measuring the induced voltage difference at the other two.
 This was performed varying the polarity and alternating the
 different pairs of probes to obtain the required number of
 measurements to obtain the sheet resistance R_s and then the
 electrical conductivity $\rho = R_s d$ (d is the thickness of the
 sample¹⁴). Finally, the stage was moved down to its original
 position and the sample removed to allow the positioning of
 the next one. All the measurements, automated and controlled
 by a computer, were performed in around 20 s. To our
 knowledge, this is the fastest power factor measurement
 reported so far. By adding the time required to place the
 sample and contact the 4 multifunctional probes by means of
 the micropositioners, a total time of 1 to 2 min could be
 expected per sample.

RESULTS AND DISCUSSION

Around 500 samples comprising single elements, binary and
 ternary alloys were initially synthesized and their power factor
 screened. From the analysis of the library of results a promising
 ternary alloy system formed by Al–Fe–Ti was identified. The
 ternary diagrams showing the Seebeck coefficient and electrical
 resistivity data are shown in Figure 3. The most negative
 Seebeck coefficient value measured was $-57 \mu\text{V/K}$, corre-
 sponding to the $\text{Al}_{12.5}\text{Fe}_{37.5}\text{Ti}_{50}$ composition (Figure 3a). Not
 very far values were observed for close compositions.

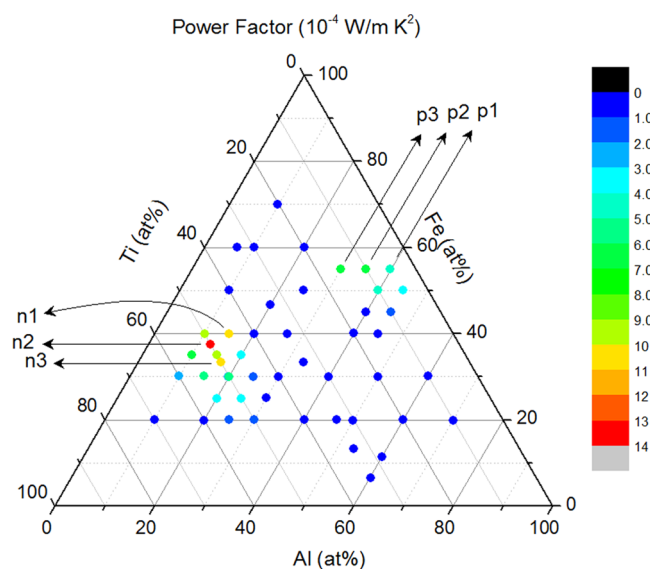


Figure 4. Results of thermoelectric screening of the power factor of the Al–Fe–Ti ternary system. Samples n1–n3 and p1–p3 are the best *n*- and *p*-type samples identified, respectively.

200 Interestingly, samples with positive Seebeck coefficient could be
 201 found when Ti content is decreased below 30%, with several
 202 compositions showing around $27 \mu\text{V}/\text{K}$. The lower Ti content
 203 of the alloys seems to be the most significant parameter
 204 affecting the transition from negative to positive Seebeck
 205 coefficients, which might cause the decrease of the mean free

206 path with the electron energy.¹⁶ It should be noted that the
 207 existence of both positive and negative values of Seebeck
 208 coefficient is highly beneficial, since both are required when the
 209 materials are assembled to form a device and this characteristic
 210 is not always present in thermoelectric bulk materials.

The electrical resistivity is shown in Figure 3b. They lie in the
 211 order of $10^{-4} \Omega \text{ cm}$, an order of magnitude lower than well-
 212 established materials such as Bi_2Te_3 . Slightly lower values were
 213 observed in the area of positive Seebeck coefficients (lower Ti
 214 content). The results of the power factor are shown in Figure 4.
 215 The highest power factor ($13.3 \times 10^{-4} \text{ W/m K}^2$) was observed
 216 in $\text{Al}_{12.5}\text{Fe}_{37.5}\text{Ti}_{50}$, corresponding to the composition of the
 217 most negative value of the Seebeck coefficient mentioned
 218 above. The highest power factor observed for positive Seebeck
 219 coefficient samples ($7.0 \times 10^{-4} \text{ W/m K}^2$) was obtained from
 220 $\text{Al}_{30}\text{Fe}_{55}\text{Ti}_{15}$. It can be seen that the large power factors are
 221 located around the above-mentioned compositions, and away
 222 from these compositions, the power factors were much lower.

223 Although the screened values of the power factor are lower
 224 than Bi_2Te_3 based alloys (typically around $30 \times 10^{-4} \text{ W/m K}^2$),
 225 they are comparable to the room temperature values of
 226 established high temperature thermoelectric materials, such as
 227 skutterudites and half heuslers. It should be noted that Al, Fe,
 228 and Ti are nontoxic and among the most earth-abundant
 229 elements of the periodic table.² Among a wide range of
 230 thermoelectric materials only silicides and oxides exhibit similar
 231 abundance. The thermal conductivity of the best samples was
 232 also measured to be in the range of 3–9 W/m K. Clearly, the
 233 Al–Fe–Ti system shows promising thermoelectric properties,
 234 which is being further investigated. 235

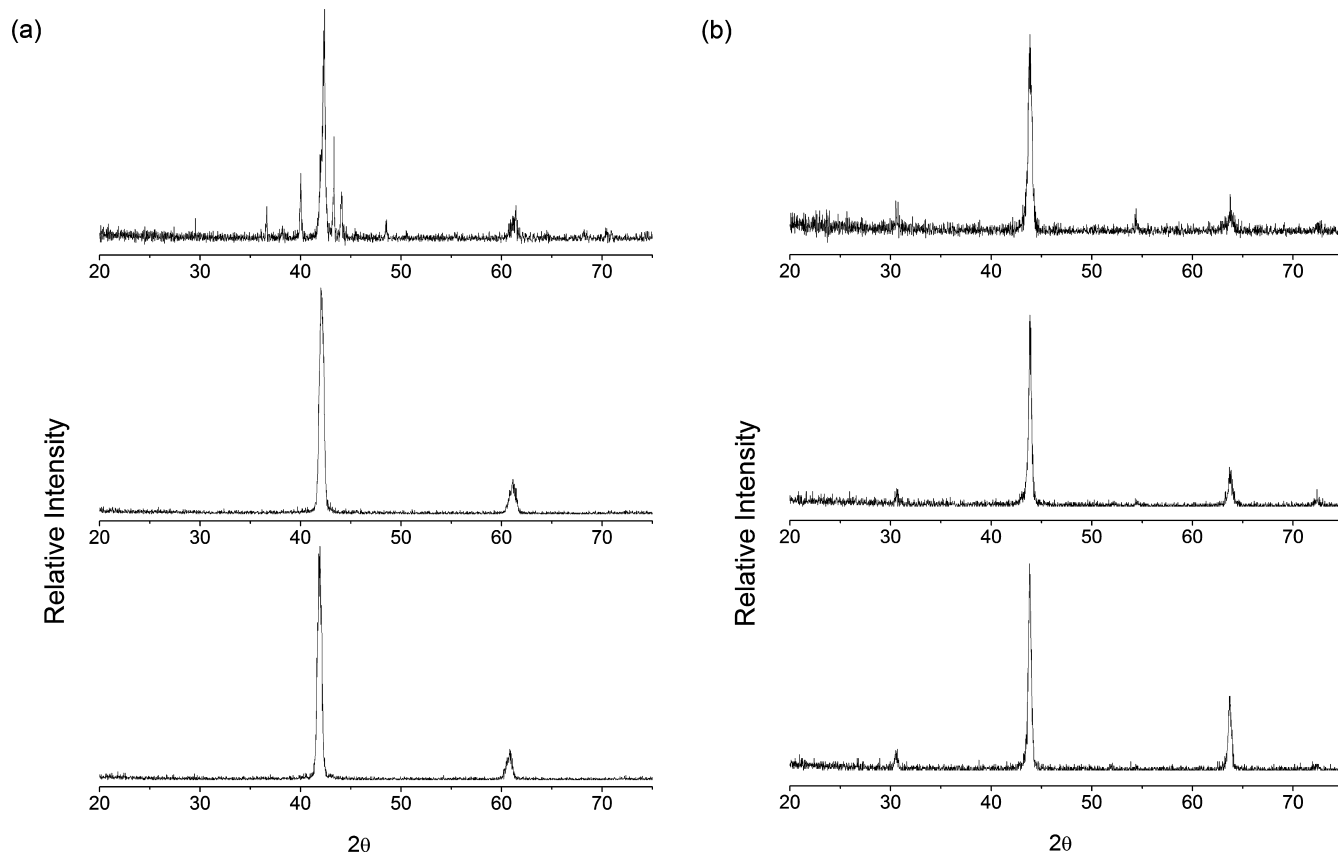


Figure 5. (a) From top to bottom, XRD of n1, n2, and n3 samples (see Figure 4). (b) From top to bottom, XRD of p1, p2, and p3 samples (see Figure 4).

236 XRD of samples with promising properties were carried out
237 to identify the crystalline phases present and to compare them
238 to those expected from literature phase diagrams. Figure 5a
239 shows the results of materials that exhibit n-type behavior,
240 whereas Figure 5b shows p-type samples. When comparing the
241 compositions of the 3 n-type materials to the isothermal
242 sections for this alloy system,¹⁷ they are expected to exhibit a
243 base centered cubic (bcc) phase but may also contain the
244 hexagonal Laves (C14) phase. The presence of two peaks at
245 42° and 61° in the XRD of n2 and n3 samples (bottom and
246 middle, Figure 5a) shows that only the bcc phase is present in
247 these materials and they exhibit A2 ordering. As there are no
248 peaks to imply B2 order, no further atomic ordering in the
249 phase of these materials can be concluded.¹⁸ Material n1 (top,
250 Figure 5a) contains an A2 bcc phase along with a minority C14
251 hexagonal phase, signified by diffraction peaks which were not
252 previously assigned to the bcc A2 phase. The presence of two
253 phases in this material is expected by considering its position on
254 the isothermal sections of this ternary system: it is located
255 between the cubic and hexagonal stable phases.¹⁷ The three p-
256 type materials have compositions which are expected to
257 crystallize to form bcc structures, as shown from the isothermal
258 sections.¹⁷ Either a disordered A2, a partially ordered B2 or full
259 Heusler bcc phase with all atoms in defined positions should be
260 expected. Our XRD results in Figure 5b imply that all three p-
261 type materials exhibit only a bcc phase. The peaks at 44° and
262 64° indicate that this phase presents at least A2 ordering, peaks
263 at 30.5°, 54.5°, and 72.5° show that B2 ordering is present and
264 no peaks for the L2₁ full Heusler phase are observed.¹⁸ The
265 above results indicate good correlation between the phases
266 identified and those expected from reported isothermal
267 sections.

268 The identification of the Al–Fe–Ti system as a promising
269 thermoelectric candidate was a surprise and the discovery of
270 both n- and p-type existing in this alloy system was completely
271 unexpected. These results demonstrate the validity of using the
272 above-reported high-throughput techniques as an effective
273 approach for accelerated discovery of thermoelectric materials.
274 They can offer the capability of high-speed discovery of
275 advanced materials, particularly among a large number of
276 ternary or quaternary intermetallic compounds.

277 ■ CONCLUSIONS

278 An integrated combinatorial approach has been developed for
279 accelerated discovery of thermoelectric materials based on a
280 laser melting technique for materials preparation and a
281 multifunctional-probe facility for thermoelectric characteriza-
282 tion. Hundreds of samples have been synthesized and their
283 room temperature power factors were characterized. This initial
284 work has led to the identification of a promising ternary system,
285 Al–Fe–Ti, which exhibits a maximum power factor of $13.3 \times$
286 10^{-4} W/m K². This value is comparable to those of the current
287 high temperature thermoelectric materials. In addition, they are
288 abundant and nontoxic and both n- and p-type exist. The
289 discovery of high power factor in Al–Fe–Ti system was
290 unexpected, which demonstrates the validity and effectiveness of
291 the high-throughput approach/techniques (reported in this
292 paper) for the development of advanced materials.

293 ■ AUTHOR INFORMATION

294 Corresponding Author

295 *E-mail: min@cardiff.ac.uk.

Present Address

296 ^{||}J.G.-C.: Department of Industrial Systems Engineering and
297 Design, Universitat Jaume I, Campus del Riu Sec, 12071
298 Castellon, Spain. 299

Author Contributions

300 The manuscript was written through contributions of all
301 authors. All authors have given approval to the final version of
302 the manuscript. 303

Funding

304 The authors wish to acknowledge financial support from the
305 Accelerated Metallurgy Project, which is cofunded by the
306 European Commission in the seventh Framework Programme
307 (contract NMP4-LA-2011-263206), by the European Space
308 Agency and by the individual partner organizations. 309

Notes

310 The authors declare no competing financial interest. 311

312 ■ ACKNOWLEDGMENTS

313 Granta Design Ltd. is acknowledged for providing the database
314 and results library. 314

315 ■ REFERENCES

- 316 (1) Martín-González, M.; Caballero-Calero, O.; Díaz-Chao, P. 316
317 Nanoengineering Thermoelectrics for 21st Century: Energy Harvest-
318 ing and Other Trends in the Field. *Renewable Sustainable Energy Rev.* 318
2013, 24 (0), 288–305. 319
- 320 (2) Gaultois, M. W.; Sparks, T. D.; Borg, C. K. H.; Seshadri, R.;
321 Bonificio, W. D.; Clarke, D. R. Data-Driven Review of Thermoelectric
322 Materials: Performance and Resource Considerations. *Chem. Mater.* 322
2013, 25 (15), 2911–2920. 323
- 324 (3) Curtarolo, S.; Hart, G. L. W.; Nardelli, M. B.; Mingo, N.; Sanvito,
325 S.; Levy, O. The High-Throughput Highway to Computational
326 Materials Design. *Nat. Mater.* 2013, 12 (3), 191–201. 326
- 327 (4) Funahashi, R.; Urata, S.; Kitawaki, M. Exploration of N-Type
328 Oxides by High Throughput Screening. *Appl. Surf. Sci.* 2004, 223 (1–
329 3), 44–48. 329
- 330 (5) Otani, M.; Lowhorn, N. D.; Schenck, P. K.; Wong-Ng, W.;
331 Green, M. L.; Itaka, K.; Koinuma, H. A High-Throughput Thermo-
332 electric Power-Factor Screening Tool for Rapid Construction of
333 Thermoelectric Property Diagrams. *Appl. Phys. Lett.* 2007, 91 (13),
334 132102. 334
- 335 (6) Watanabe, M.; Kita, T.; Fukumura, T.; Ohtomo, a.; Ueno, K.;
336 Kawasaki, M. Combinatorial Synthesis and High Throughput
337 Evaluation of Thermoelectric Power Factor in Mg-Si-Ge Ternary
338 Compounds. *Appl. Surf. Sci.* 2007, 254 (3), 777–780. 338
- 339 (7) Potyrailo, R.; Rajan, K.; Stowe, K.; Takeuchi, I.; Chisholm, B.;
340 Lam, H. Combinatorial and High-Throughput Screening of Materials
341 Libraries: Review of State of the Art. *ACS Comb. Sci.* 2011, 579–633. 341
- 342 (8) Hautier, G.; Jain, A.; Ong, S. P. From the Computer to the
343 Laboratory: Materials Discovery and Design Using First-Principles
344 Calculations. *J. Mater. Sci.* 2012, 47 (21), 7317–7340. 344
- 345 (9) Bera, C.; Jacob, S.; Opahle, I.; Gunda, N. S. H.; Chmielowski, R.;
346 Dennler, G.; Madsen, G. K. H. Integrated Computational Materials
347 Discovery of Silver Doped Tin Sulfide as a Thermoelectric Material. 347
Phys. Chem. Chem. Phys. 2014, 16, 19894–19899. 348
- 349 (10) Carrete, J.; Li, W.; Mingo, N.; Wang, S.; Curtarolo, S. Finding
350 Unprecedentedly Low-Thermal-Conductivity Half-Heusler Semicon-
351 ductors via High-Throughput Materials Modeling. *Phys. Rev. X* 2014,
352 4, 011019. 352
- 353 (11) Yan, J.; Gorai, P.; Ortiz, B.; Miller, S.; Barnett, S. a.; Mason, T.;
354 Stevanović, V.; Toberer, E. S. Material Descriptors for Predicting
355 Thermoelectric Performance. *Energy Environ. Sci.* 2015, 8, 983–994. 355
- 356 (12) Yan, Y. G.; Martin, J.; Wong-Ng, W.; Green, M.; Tang, X. F. A
357 Temperature Dependent Screening Tool for High Throughput
358 Thermoelectric Characterization of Combinatorial Films. *Rev. Sci.* 358
Instrum. 2013, 84 (11), 115110. 359

- 360 (13) Watanabe, M.; Kita, T.; Fukumura, T.; Ohtomo, A.; Ueno, K.;
361 Kawasaki, M. High-Throughput Screening for Combinatorial Thin-
362 Film Library of Thermoelectric Materials. *J. Comb. Chem.* **2008**, *10*
363 (2), 175–178.
- 364 (14) García-Cañadas, J.; Min, G. Multifunctional Probes for High-
365 Throughput Measurement of Seebeck Coefficient and Electrical
366 Conductivity at Room Temperature. *Rev. Sci. Instrum.* **2014**, *85* (4),
367 043906.
- 368 (15) Van der Pauw, L. J. A Method of Measuring Specific Resistivity
369 and Hall Effect of Discs of Arbitrary Shape. *Philips Res. Reports* **1958**,
370 *13* (1), 1–9.
- 371 (16) Kasap, S. O. *Thermoelectric Effects in Metals: Thermocouples*;
372 University of Saskatchewan: Saskatchewan, Canada, 2001
- 373 (17) Palm, M.; Lacaze, J. Assessment of the Al–Fe–Ti System.
374 *Intermetallics* **2006**, *14* (10–11), 1291–1303.
- 375 (18) Yin, M.; Hasier, J.; Nash, P. A Review of Phase Equilibria in
376 Heusler Alloy Systems Containing Fe, Co or Ni. *J. Mater. Sci.* **2016**, *51*
377 (1), 50–70.